Behavior of Periodic Coupled Microstrip Resonators

Author: Jack Timpson Wimberley

Behavior of Periodically Spaced Coupled Microstrip Resonators

Jack Wimberley

Department of Physics
Boston College
Bachelor of Science

Prof. Kris Kempa, Advisor

May 2011

Abstract

The resonant modes of a sequence of periodically spaced microstrip resonators is studied. The system is analyzed as transmission line with periodic capacitive gaps, as a waveguide with apertures via normal mode expansion, and through a derivation of the static fields in the gap between two microstrip resonators via conformal mapping. FDTD simulations are also performed to numerically calculate the resonant modes of the sequence and also its absorption spectrum when it contains a lossy dielectric. It is found, as expected, that when the gap size is large, the microstrip resonators are uncoupled and there resonant modes are unperturbed. As the gap size narrows, the resonators become strongly coupled, and changing boundary conditions perturb the resonant modes upwards in frequency. Moreover, an additional resonant mode is observed that does not correspond to any uncoupled mode.

Acknowledgements

I would like to thank the faculty of the physics department, especially Prof. Kris Kempa, who took me on as an undergraduate researcher my sophomore year, and Prof. Michael Graf. I also thank Alec Rose ('09) and Yun Peng, who introduced me to research tools such as Meep used in this project, and the faculty of the mathematics department, including Prof. C. K. Cheung and Prof. William Keane.

Contents

List of Figures

Chapter 1

Introduction

1.1 Motivation

Research during the summers of 2009 and 2010 with Prof. Kris Kempa in designing broadband near perfect absorbers was successful and brought up several areas of possible further research. The experimental configuration for a near perfect absorber, conceived as a method of increasing the efficiency of a solar cell, is shown in Fig. 1.1. This design consists of a microstrip resonator that traps incoming solar radiation in a lossy dielectric. A lattice of such microstrip resonators of varying sizes and orientations could then be used to create a functional broadband perfect absorber.

The analysis of such a lattice assumed uncoupled microstrip resonators, which behave largely like rectangular cavity resonators. However, computer simulations showed that there is in fact strong coupling between neighboring microstrip resonators when they are spaced close together. It is sufficient to consider a 1D lattice or sequence of microstrip resonators to study this coupling. In Fig. 1.1, s is the distance between two the corresponding edges of two resonators, i.e. the unit size of the periodic sequence. The variable l is the length of each resonator; the ratio s/l measures the ratio of the size of the unit cell to the size of the resonator and $d = s - l$ is the width of the gap between neighboring resonators. Fig. 1.2 shows some of the results of simulation. In this plot ω is the resonant frequency of the system, determined by finding the frequency of maximum absorption in the simulation. It was found that as the ratio s/l increases and the resonators become decoupled, ω rapidly converges to a value ω_0, as expected since in this limit coupling becomes unimportant. This frequency

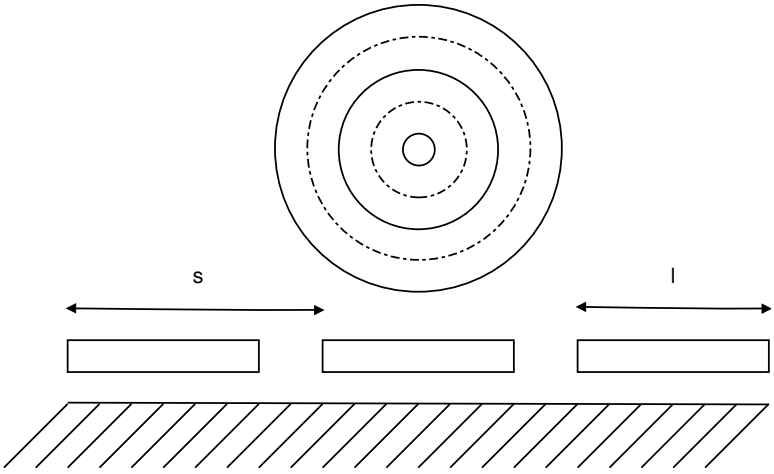

Figure 1.1: A lattice of rectangular microstrips atop a dielectric and metallic substrate traps incoming solar radiation to increase the efficiency of a solar cell.

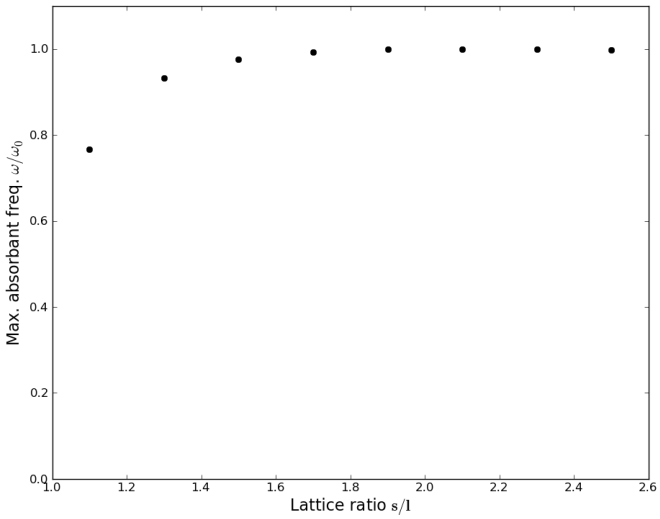

Figure 1.2: The resonant frequency of the microstrip resonator appears to decrease as it is brought closer to and couples more strongly to its neighbors.

ω_0, moreover, corresponds to a resonant mode of the microstrip resonator. In the other limit, as the microstrip resonators become closely spaced together, ω decreases significantly, indicating strong coupling. Analyzing this coupling in greater detail will provide insight into the behavior of the resonant absorber system, and could lead to ways of optimizing the

efficiency of a broadband perfect absorber.

1.2 Analytical Methods

This problem can be approached using several computational and analytical methods. The original simulation modeled a three dimensional photovoltaic cell, and featured gold microstrips and a lossy silicon dielectric, and found resonances in the lossy structure by computing transmission spectra and finding absorption peaks. This problem would be intractable to solve analytically. A simpler model to study eliminates one of the spatial dimensions (the normal in Fig. 1.1), which is justified since all the important spatial variation in the problem is in the given plane). Additionally, replacing the lossy metal and silicon with a perfect conductor and perfect dielectric will great simplify the problem, which can then be approached by finding the behavior of resonant modes rather than the transmission spectra. A set of computer simulation will demonstrate that these resonant modes correspond roughly to the absorption peaks in a simulation of a lossy system (radiation is trapped at the resonances and with a longer mean free path in the lossy material, more is absorbed). This simpler model system can be studied analytically using tools from basic electromagnetic theory, waveguide theory, and transmission line and microwave network theory. These tools include model two ports, equivalent circuit representations, normal mode analysis, and conformal mapping. All these results can be compared to data from computer simulations.

1.3 Resonant LC Circuit

A quick and dirty approach to modeling the coupled microstrip resonators treats them as LC circuits. The fundamental mode of a microstrip resonator is represented as that of an LC circuit, with frequency $1/\sqrt{LC}$. As the microstrip sits atop the conducting ground plate,

it behaves naively like a parallel plate capacitor. For a microstrip with length l (in the direction of coupling), width w, and height h above the ground plate, and a dielectric with ϵ and μ, this capacitance is roughly $C = \epsilon wl/h$. The inductance of the microstrip, meanwhile, is a property of the raised strip, and should be proportional to the length l and inversely proportional to the width w (in analogy with the resistance of a finitely sized conductor). Knowing furthermore that the inductance is a magnetic effect, we can hand waive and say that it is $L = \mu hl/w$. Then the fundamental frequency is

$$\omega_0 = \frac{1}{\sqrt{LC}} = \frac{1}{\sqrt{\mu\epsilon}}\frac{1}{l} = \frac{c}{nl}$$

It makes similar sense to treat the gaps between neighboring resonators as capacitors. If the thickness of the resonator is t and the distance between resonators is d, then this capacitance is $C_g = \epsilon' wt/d$, where ϵ' is an effective dielectric constant. In terms of C, this is

$$\frac{C_g}{C} = \left(\frac{\epsilon'}{\epsilon}\right)\frac{ht}{ld} = \left(\frac{\epsilon'}{\epsilon}\frac{ht}{l^2}\right)\frac{1}{r-1},$$

where $r = s/l = d/l + 1$ is the dimensionless ratio of the periodicity length to the resonator length. Ignoring the lossy effects of the gaps between the resonators, the effect of the capacitance can be accounted for in a very rough sense by adding an extra capacitor in parallel to the LC circuit model. The resonant frequency of the circuit is then shifted to

$$\omega = \frac{1}{\sqrt{L(C+C_g)}} = \frac{\omega_0}{\sqrt{1+C_g/C}} = \omega_0\sqrt{\frac{r-1}{r-1+\alpha}}, \tag{1.1}$$

where α is a constant. Assuming $\epsilon' \simeq \epsilon$, the numerical parameters used in the simulation of Fig. 1.2 are $l = 1\mu\text{m}$, $w = 0.35\mu\text{m}$, $h = 0.185\mu\text{m}$, and $t = 0.1\mu\text{m}$, giving $\alpha \simeq 0.0185$. This prediction can be plotted against the data in Fig. 1.2. As shown in Fig. 1.3, this model is not in great agreement with data. This can be improved numerically by adjusting the value

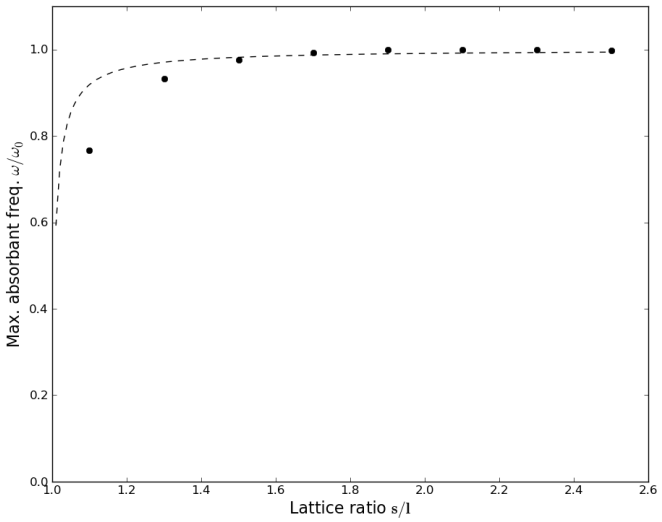

Figure 1.3: The LC circuit model fails to account for the behavior of the coupled resonant strips.

of the constant α, but doing so eliminates the physical motivation for the model (α must be adjusted by nearly an order of magnitude) and the end result predicts much greater coupling at longer separations than simulation shows. Moreover, it makes more intuitive sense to add the capacitor to the circuit in series, which gives different predictions that do not agree at all with these simulations.

Chapter 2

Review

Transmission lines and waveguides are well studied topics of electromagnetism and electrical engineering. In principle, the two concepts are not very different. Both transmission lines and waveguides are devices used to propagate electromagnetic energy, usually along metallic guides. Such a device tends to be called a transmission line when dealing with low frequency electromagnetic waves such as radio waves or microwaves, in which case it is treated analytically as an extended electric circuit. When dealing with higher frequencies waves closer to the optical spectrum, such a device is called a waveguide and is studied by directly applying Maxwell's equations. The distinction is not very clear cut, and two approaches are both useful. The simplified equivalent circuit treatment of a transmission line is not able to describe the normal modes of an unterminated line, for example, but is better equipped to study discontinuities in the line by modeling them as impedances. A further difference is that waveguide theory is equipped to study propagating TE and TM modes down a line, while the transmission line theory is only equipped to study TEM modes [6, pp. 218-219]. Both types of analysis will be useful in studying the sequence of microstrip resonators. A microstrip resonator is simply a finite section of a microstrip transmission line, which consists of a rectangular metallic strip atop a dielectric and metal substrate. Microstrips are an important class of transmission line, and have been studied intensely, but for our purposes it is not important to delve too deeply into their intricacies.

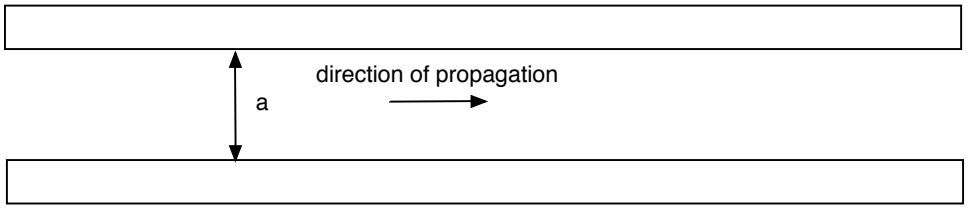

Figure 2.1: A parallel plate waveguide propagates electromagnetic waves between two conducting surfaces.

2.1 Waveguides

Instead, consider a two dimensional parallel plate waveguide, such as the one shown in Fig. 2.1. Define z to be the direction of propagation, x to be the vertical (top of the page), and y to be the normal (out of the page). The behavior of this waveguide can be found easily using Maxwell's equations. Note that a complete solution in fact treats a 3D waveguide with rectangular cross section [1, p. 361]. This extra complication is unnecessary here, as will be discussed later. An electromagnetic wave with time dependence $\exp(-i\omega t)$ propagating in the interior of this waveguide obeys Maxwell's equations for empty space [1, 8.16]:

$$\begin{aligned} \boldsymbol{\nabla} \times \mathbf{E} &= i\omega \mathbf{B} & \boldsymbol{\nabla} \cdot \mathbf{B} &= 0 \\ \boldsymbol{\nabla} \times \mathbf{B} &= -i\mu\epsilon\omega \mathbf{E} & \boldsymbol{\nabla} \cdot \mathbf{E} &= 0 \end{aligned} \tag{2.1}$$

Finding the modes that travel in this waveguide is simply a matter of following Jackson's work in two dimensions rather than three. If we look for wave solutions of the form $\mathbf{E}(x, z, t) = \mathbf{E}(x) \exp(\pm kz - i\omega t)$, and similarly for $\mathbf{B}$, fields satisfying the equations 2.1 necessarily satisfy

$$\left(\boldsymbol{\nabla}_x^2 + \left(\mu\epsilon\omega^2 - k^2\right)\right) \left\{ \begin{array}{c} \mathbf{E} \\ \\ \mathbf{B} \end{array} \right\} = 0, \tag{2.2}$$

where $\boldsymbol{\nabla}_x$ is the $\partial/\partial x$ operator (in assuming that the waveguide is 2D, we assume that there is no variation in the fields in the y direction) [1, 8.19-20]. This equation treats each

of the components of E and B separately. Recall that we are considering the wave to be propagating in the positive z direction. It can be derived from (2.1) that if either $E_z \neq 0$ or $B_z \neq 0$, the transverse components of the electric and magnetic fields are given in terms of the z components by [1, 8.26]

$$\mathbf{E}_t = \frac{i}{\mu\epsilon\omega^2 - k^2}\left(\pm k\frac{\partial E_z}{\partial x}\hat{\mathbf{x}} - \omega\frac{\partial B_z}{\partial x}\hat{\mathbf{y}}\right) \tag{2.3}$$

$$\mathbf{B}_t = \frac{i}{\mu\epsilon\omega^2 - k^2}\left(\pm k\frac{\partial B_z}{\partial x}\hat{\mathbf{x}} + \mu\epsilon\omega\frac{\partial E_z}{\partial x}\hat{\mathbf{y}}\right). \tag{2.4}$$

It is apparent that the wave must be a superposition of two classes of simpler modes. These are the the transverse magnetic (TM) mode, in which the magnetic field is completely transverse to the direction of propagation (i.e. $B_z = 0$), and similarly the transverse electric (TE) mode. In each case, the tangential fields are completely determined by the normal electric or magnetic field component. It is traditional at this point to use the field $\mathbf{H}$ rather than $\mathbf{B}$. The tangential components of a TM mode are given in terms of E_z by

$$\begin{aligned} E_x &= \frac{\pm ik}{\mu\epsilon\omega^2 - k^2}\frac{\partial E_z}{\partial x} & E_y &= 0 \\ H_x &= 0 & H_y &= \frac{i\epsilon\omega}{\mu\epsilon\omega^2 - k^2}\frac{\partial E_z}{\partial x} \end{aligned} \tag{2.5}$$

It is often useful to remember that the tangential electric and magnetic fields are related to each other by the TM impedance $Z_{TM} = k/\epsilon\omega$:

$$\mathbf{H}_t = \frac{\pm 1}{Z_{TM}}\hat{\mathbf{z}} \times \mathbf{E}_t \tag{2.6}$$

The normal component E_z satisfies equation (2.2) and moreover has boundary conditions $E_z|_S = 0$, since the boundary is a metallic surface. Defining $\gamma^2 = \mu\epsilon\omega^2 - k^2$, this is an eigenvalue equation $\nabla_x^2 E_z = -\gamma^2 E_z$ where $E_z(0) = E_z(a) = 0$. The eigensolutions to this

equation are

$$E_z = \sin(\gamma_m x), \tag{2.7}$$

where m is an integer ≥ 1 and $\gamma_m = m\pi/a$. Note that this means that propagation of the wave is given by $k_m = \sqrt{\mu\epsilon\omega^2 - \gamma_m^2}$, and that there is a cutoff frequency $\omega_m = \gamma_m/\sqrt{\mu\epsilon}$ below which the mth mode will not propagate. Substituting this into (2.5), we see that the transverse fields are

$$E_x = \frac{\pm ika}{m\pi}\cos\left(\frac{m\pi x}{a}\right), \quad H_y = \frac{i\epsilon\omega a}{m\pi}\cos\left(\frac{m\pi x}{a}\right) \tag{2.8}$$

The $\pm i$ factor in E_x signifies that this component is a quarter cycle out of phase with E_z in the z direction, while the i factor in H_y signifies that this is a quarter cycle out of phase with E_z in time. The tangential components of a TE mode are given in terms of H_z by

$$\begin{aligned} E_x &= 0 & E_y &= \frac{-i\mu\omega}{\mu\epsilon\omega^2 - k^2}\frac{\partial H_z}{\partial x} \\ H_x &= \frac{\pm ik}{\mu\epsilon\omega^2 - k^2}\frac{\partial H_z}{\partial x} & H_y &= 0 \end{aligned} \tag{2.9}$$

In analogy with (2.6), we define $Z_{TE} = \mu\omega/k$, and the electric and magnetic tangential components are related by

$$\mathbf{H}_t = \frac{\pm 1}{Z_{TE}}\hat{\mathbf{z}} \times \mathbf{E}_t \tag{2.10}$$

The normal magnetic field B_z satisfies (2.2) and has boundary conditions $\partial H_z/\partial n|_S = 0$. The is an eigenvalue equation in this case is $\nabla_x^2 H_z = -\gamma^2 H_z$ where $H_z'(0) = H_z'(a) = 0$. The eigensolutions to this equation are

$$H_z = \cos(\gamma_m x), \tag{2.11}$$

where m is an integer ≥ 0 and again $\gamma_m = m\pi/a$. The transverse fields are given by

$$E_y = \frac{i\mu\omega a}{m\pi} \sin\left(\frac{m\pi x}{a}\right), \quad H_x = \frac{\mp ika}{m\pi} \cos\left(\frac{m\pi x}{a}\right) \tag{2.12}$$

In the case that both $E_z = 0$ and $B_z = 0$, equations (2.3) and (2.4) do not hold. In this case a degenerate type of wave called, naturally, a TEM wave is in general possible. For such a wave $\boldsymbol{\nabla}_x \times \mathbf{E}_{TEM} = 0$ and $\boldsymbol{\nabla}_x \cdot \mathbf{E}_{TEM} = 0$, meaning that the electric field in the cross section of the waveguide is an electrostatic solution to the boundary conditions given by the waveguide [1, p. 360]. In the present case, the two parallel plates are equipotential surfaces, so the electric (and consequently magnetic) fields between them can take static values [6, p. 399]. However, a TEM mode is not always possible for other types of waveguides in which the metallic boundaries are disconnected and where there are non-metallic boundaries, such as for the microstrip transmission line.

Equations (2.7) - (2.12) fully describe the modes of the parallel plate transmission line. Using these equations to describe the behavior of a microstrip transmission line is in fact the lowest-order tenable approximation [6, p. 411]. Much more complicated methods have been used to describe the properties of a true microstrip transmission line [7]; however, most of these results are outside the scope of this thesis. One notable result is that the microstrip transmission line supports a quasi TEM mode, since the electric field is not forced to be simultaneously zero on all edge faces of the transmission line. In the more precise treatments mentioned above, this quasi TEM mode is usually identified with the lowest order TE or TM of the the approximate parallel plate transmission line.

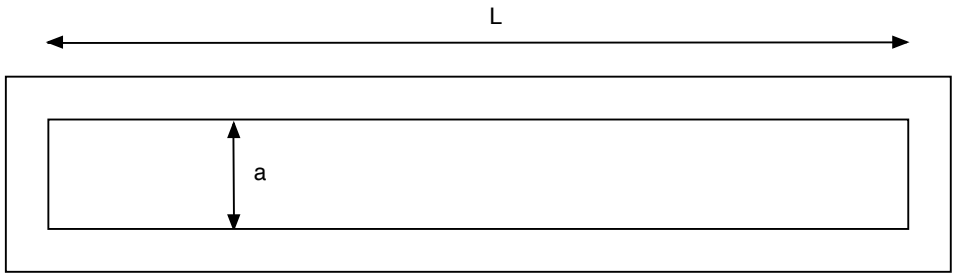

Figure 2.2: A 2D rectangular cavity resonator is a terminated section of a parallel plate waveguide.

2.2 Cavity Resonators

When a microstrip transmission line is terminated to a finite length roughly comparable to the wavelength of the radiation it supports, it becomes a lossy resonant cavity. With its rectangular dimensions, the microstrip resonator is a variant of a rectangular resonant cavity. Consider a 2D rectangular cavity with dimensions (a, L) in the (x, z) directions, as shown in Fig. 2.2. This is simply a portion of a parallel plate waveguide with conducting plates at $z = 0$ and $z = L$. So, its resonant TM and TE modes (which are superpositions of the forwards and backwards propagating modes of the parallel plate waveguide) must have their transverse electric fields take the value 0 at these two faces. The first consequence of this is that the propagation factor k must be an integer multiple of π/L, i.e. $n\pi L$, just as γ_m was constrained to be an integer multiple of π/a. Consequently, the related constants γ_m and ω are restricted. In summary, the mode is described by two integer parameters m and n such that

$$\mu\epsilon\omega_{mn}^2 = \gamma_m^2 + k_n^2 = \left(\frac{m\pi}{a}\right)^2 + \left(\frac{n\pi}{L}\right)^2 \tag{2.13}$$

It is clear now that a resonant mode is completely described by three pieces of information: a) whether it is TM or TE, b) its value of m, and c) its value of n. A convenient symbol for a particular mode, therefore, is TM_{mn} or TE_{mn}, as the case may be. Since TM and TE

modes with identical m and n are degenerate in this case (and most others), a mode will often be labelled simply as mn when there is no confusion whether it is a TM or TE mode or when this distinction is unimportant. This notation is not ambiguous, since the modes considered in this thesis will never reach into the double digits.

Inspecting (2.7) and (2.8), we see that transverse electric fields in the TM case are a quarter period out of phase with E_z (because of the $\pm i$), and so they are zero when E_z is at a local maximum on the edge faces. Evidently, E_z varies with z as $\cos(k_n z)$ and the other fields are in phase or out of phase as required. So, the field components of a TM_{mn} mode are given by

$$E_x = \frac{na}{mL}\cos\left(\frac{m\pi x}{a}\right)\sin\left(\frac{n\pi z}{L}\right) \tag{2.14}$$

$$H_y = \frac{i\epsilon\omega a}{m\pi}\cos\left(\frac{m\pi x}{a}\right)\cos\left(\frac{n\pi z}{L}\right) \tag{2.15}$$

$$E_z = \sin\left(\frac{m\pi}{a}\right)\cos\left(\frac{n\pi z}{L}\right) \tag{2.16}$$

For a TE_{mn} phase, (2.11) and (2.12) show that the tangential electric field is in phase with H_z (the i is a time phase), and the resulting components of the mode are given by

$$H_x = \frac{na}{mL}\cos\left(\frac{m\pi x}{a}\right)\cos\left(\frac{n\pi z}{L}\right) \tag{2.17}$$

$$E_y = \frac{i\mu\omega a}{m\pi}\sin\left(\frac{m\pi x}{a}\right)\sin\left(\frac{n\pi z}{L}\right) \tag{2.18}$$

$$H_z = \cos\left(\frac{m\pi}{a}\right)\sin\left(\frac{n\pi z}{L}\right) \tag{2.19}$$

A microstrip resonator behaves like a rectangular resonator, but with fringing fields at the ends and sides where it has open (rather than metallic) boundary conditions (see Fig. 2.3. This can be accounted for heuristically by (1) assuming that the resonator has slightly perturbed effective dimensions and (2) ensuring zero tangential magnetic field at the

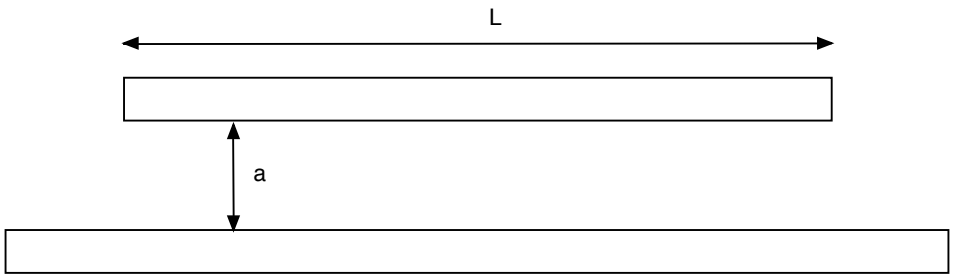

Figure 2.3: A 2D microstrip resonator has open boundary conditions.

boundaries [6, pp. 501]. Call the perturbed dimensions of the microstrip $a' = a + \delta a$ and $L' = a + \delta L$. For a TM mode, repeating the above arguments with these new boundary conditions gives the components of the TM_{mn} mode of the (2D) microstrip resonator:

$$E_x = \frac{na'}{mL'} \cos\left(\frac{m\pi x}{a'}\right) \cos\left(\frac{n\pi z}{L'}\right) \tag{2.20}$$

$$H_y = \frac{i\epsilon\omega a'}{m\pi} \cos\left(\frac{m\pi x}{a'}\right) \sin\left(\frac{n\pi z}{L'}\right) \tag{2.21}$$

$$E_z = \sin\left(\frac{m\pi}{a'}\right) \sin\left(\frac{n\pi z}{L'}\right) \tag{2.22}$$

The components of the TE_{mn} mode of a microstrip resonator are

$$H_x = \frac{na'}{mL'} \cos\left(\frac{m\pi x}{a'}\right) \sin\left(\frac{n\pi z}{L'}\right) \tag{2.23}$$

$$E_y = \frac{i\mu\omega a'}{m\pi} \sin\left(\frac{m\pi x}{a'}\right) \cos\left(\frac{n\pi z}{L'}\right) \tag{2.24}$$

$$H_z = \cos\left(\frac{m\pi}{a'}\right) \cos\left(\frac{n\pi z}{L'}\right) \tag{2.25}$$

The literature treats actual three dimensional microstrip resonators, such as in [6, pp. 500-501]. Here, there are also open boundary conditions on the side faces (in the xy plane) of the microstrip resonator. The literature states that this further restricts the possible behavior of the resonator. One consequence is that the modes of the microstrip resonator must be TE and cannot have variation in the x direction (i.e. $m = 0$; also note that the

literature uses different axes). Neither of these applies to the 2D microstrip resonator, and in fact $m = 0$ modes will not be studied because (as will be explained later) they were difficult to excite using FDTD simulation software. However, the remainder of the thesis will concentrate on TE modes.

2.3 Transmission Lines

An alternative method of studying transmission lines treats them as extended electric circuits. Since light is an electromagnetic wave, the radiation confined to propagate down a transmission line is in principle very similar to sinusoidally varying electric waves traveling through a circuit. The literature on these techniques is very well developed (see [2] and [6]) and, unlike the waveguide and resonator modes reviewed above, this background is not needed to interpret the results of the simulations described later. However, several techniques from this literature are used in analysis. Here is a brief review of the principles behind the equivalent circuit techniques used in the study of transmission lines.

A transmission line (such as a microstrip transmission line) propagating fields in the direction z can be modeled as an extended circuit with voltage $V(z)$ and current $I(z)$, rather than directly using Maxwell's equations to study E and B. A simple line consisting of two parallel conductors, for example, is assumed to have a distributed inductance L and capacitance C per unit length. Then a differential element of the transmission line behaves like a small two port circuit element with series inductance $L\,dz$ and parallel (or shunt) capacitance $C\,dz$. The behavior of the transmission is described by Heaviside's Telegrapher's

Equations [6, pp. 214-5]:

$$\frac{\partial V}{\partial z} = -L\frac{\partial I}{\partial t}$$
$$\frac{\partial I}{\partial z} = -C\frac{\partial V}{\partial t}$$

The analysis of these equations reveals that the most important parameter describing propagation on the transmission line is its characteristic impedance [6, p. 217], defined as

$$Z_0 = \sqrt{\frac{L}{C}}$$

This can be generalized to more complicated waveguides by considering alternative differential elements, containing extra series or shunt losses, inductances, or capacitances. Alternatively, transmission lines where the basic two port units are discrete chunks and not differentials can be studied with matrix techniques. More importantly, defects, obstacles, or other discontinuities (standalone or periodic) in the transmission line can themselves be modeled as circuit elements, and matrix techniques can be used to analyze their effects. Later, the gaps between neighboring microstrip resonators will be treated as periodic series capacitive elements on a transmission line, and use some of these techniques will be employed to study the their effect on the transmission line.

Chapter 3

Numerical Simulation

3.1 Resonator Modes

The program Meep is an open source open source FDTD electromagnetic simulation project developed at MIT [5]. It is capable of modeling dielectric, metallic, and lossy media in several dimensions and computing transmission spectra and resonant modes (using a specialized algorithm [3] that is a variant of a Fourier transform).

Meep's accuracy can be demonstrated by using it to calculate the resonant frequencies of a 2D rectangular resonator filled with a vacuum. Several difficulties were encountered while performing these simulations. First, only modes with odd values of m and n were excited because these all share a common node in the geometric center of the resonator. The even labeled modes do not in general share a common node with each other or with the odd numbered modes, and so it is generally much easier to excite multiple odd modes simultaneously (simply by placing a point source in the center) than even modes. Second, exciting TE modes in Meep was more reliable than exciting TM modes, for unknown reasons. The TE_{11} mode was the lowest order mode of the rectangular cavity resonator or microstrip resonator that could be reliably studied using Meep, and so for the purposes of this research this was effectively the fundamental mode.

Meep uses dimensionless units in which c, μ_0, and ϵ_0 are all equal to 1. The program takes advantage of the scale invariance of the equations of electromagnetism by reporting distance in multiples of some arbitrary unit length a. Correspondingly, frequency is reported in units of $2\pi c/a$ (cyclical frequency rather than angular frequency). The simulation file used for this test is given in the appendix (A.1). This simulation describes a 2D rectangular resonator

Mode	Calculated Frequency	Meep Error
1x1	0.128846490613857	4.47612618237562e-6
1x3	0.156240803293938	4.80319514495409e-7
1x5	0.200122142332131	7.38085104600644e-6
1x7	0.251862861842301	2.57585377387968e-6
1x9	0.307724322870505	1.81950335916637e-6
1x11	0.363651067905817	2.65983802340615e-4
3x1	0.374275045285169	7.32461359363812e-4
3x3	0.389307662941443	0.00121686619537507

Figure 3.1: Frequencies of several TE modes of 2D rectangular resonator

with dimensions 4 and 16 (again in units a, where the value of a does not matter). The resonant frequencies should be exactly as given by (2.13) with $x = 4a$ and $y = 16a$. In Meep's units the frequency of the 11 mode, for example, should be

$$f = \frac{1}{2}\sqrt{\left(\frac{1}{4}\right)^2 + \left(\frac{1}{16}\right)^2} = \frac{\sqrt{17}}{32} = 0.1288470508$$

The resonant frequencies and corresponding errors calculated by Meep are listed in Fig. 3.1, where "Mode 1x1" denotes TE_{11}, etc. Meep runs a harmonic inverse algorithm to find the frequencies of the normal modes, and their corresponding modes can be found by outputting a graphical representation of the field intensity from within Meep. Fig. 3.2 shows time slices of the transverse electric field intensity for three separate modes. The frequencies obtained by Meep agree with theory quite well, with error generally 1 part in 10^4 or lower. The simulated frequencies for the highest order modes are off by close to one part in a hundred, but for these modes Meep indicated a higher internal error than in lower modes. Across the board, Meep's estimation of its error is too low, but overall its performance is still more than adequate.

The next step is to use Meep to find the resonant modes of a microstrip resonator and

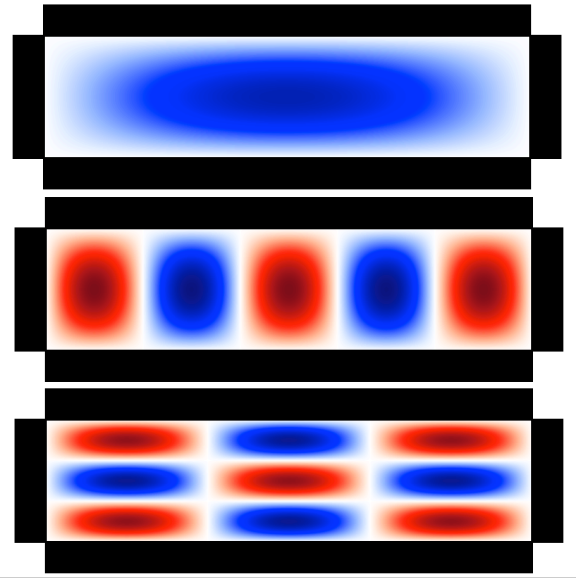

Figure 3.2: Modes of the rectangular resonator. From top to bottom: TE_{11}, TE_{15}, TE_{33}.

compare these to theory. Recall that literature states that the modes of a microstrip resonator should correspond to the the TE modes of the corresponding rectangular cavity with extended effective dimensions and with no x variation (i.e. $m = 0$). As mentioned, it was difficult to perform simulations that could observe $m = 0$ modes. The file used for this simulation is shown in Appendix A.2. The justification given in the literature that $m \neq 0$ modes should not exist is that there should be zero tangential magnetic fields at the sides of the microstrip, which is an idealization. In the Meep simulation the 11 mode appears at the frequency (in Meep units) $\omega = 0.127466$. The effective length of the resonator in this simulation is

$$\frac{L_{eff}}{L} = \frac{\omega_0}{\omega} = \frac{0.128846}{0.127466} \simeq 1.011 \tag{3.1}$$

This resonant mode is clearly analogous to the 11 mode of the rectangular cavity, as shown in Fig. 3.3. Visually, the "length" of the resonance appears to be more than 1.1% greater than the length of the microstrip, but as an abstraction of the more complicated boundary conditions in this problem, the effective length does not correspond to a geometric length.

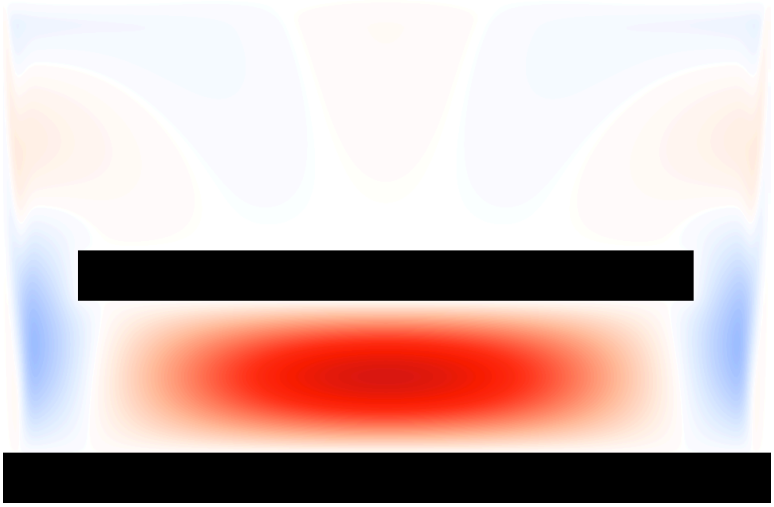

Figure 3.3: The TE_{11} mode of the resonator (the magnitude of E_y is plotted) is clearly analogous to the equivalent rectangular cavity mode, but it is lossy and radiates away energy. The sharp changes in the fields seen on the left and right sides are an artifact of Meep's use of PML to represent semi-infinite vacuums.

It is immediately clear that the magnitude of E_y is proportional to $\sin k_n z$ for some k_n, since E_y reaches its maximum in the middle of the resonator and its minimum at the fringe edges. This contradicts (2.23) - (2.25), which were derived from the open boundary conditions listed in the literature. These boundary conditions are clearly not correct in this instance. They possibly hold for the 3D microstrip resonator but not for the 2D microstrip simulated here. Alternatively, the analysis in [6] described the boundary conditions of the microstrip resonator when it is coupled to a transmission line (evidence for this will be shown below).

3.2 Coupled Resonator Modes

The behavior of the system once coupling between neighboring microstrip resonators is introduced can be numerically by taking the same geometry as before but requiring the fields to be translationally periodic. The effect of this periodicity is that the fields are exactly those

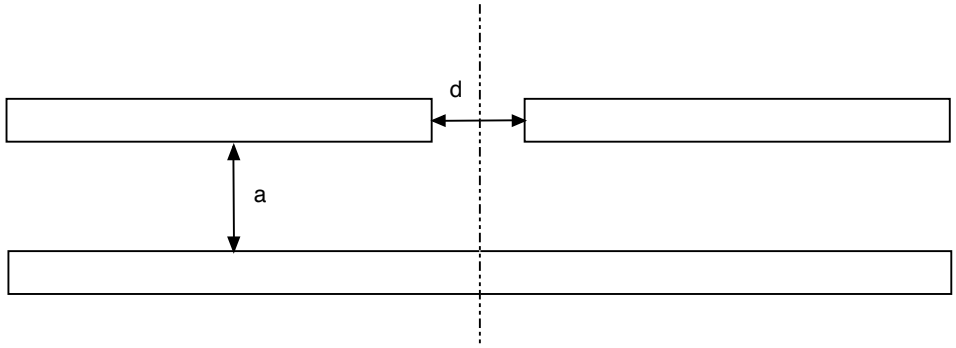

Figure 3.4: The gap between neighboring microstrip resonators creates new boundary conditions.

that would be caused by the periodic geometry shown in Fig. 3.4. The simulation file to find the resonant modes of this geometry is given in Appendix A.3. The frequencies of the resonant (TE) modes are plotted as a function of the ratio s/l in Figs. 3.5. The results are not at all what was expected. Instead of the resonant frequency decreasing with the lattice ratio s/l, as seemed to occur in the simulations conducted in previous research, the modes actually increased in frequency. In fact, for the lowest modes, there appears to be a clear pattern. The coupled 11 mode increases in frequency and converges towards the uncoupled 12 mode as $s/l \to 0$. Additionally, a resonant mode that is not expected based on analogy to a rectangular cavity appears as s/l decreases (presumably once its Q factor becomes high enough for it to be observed) and converges towards the uncoupled 10 mode as $s/l \to 0$. Some images of the electric fields in these modes can aid interpretation of these effects. Consider the 11 mode first. When s/l is large, this mode is essentially that shown in Fig. 3.3. As s/l decreases, it shifts as shown in Fig. 3.6 and Fig. 3.7.

It is visually apparent what occurs during this transition. As the coupling between neighboring resonators becomes strong, the boundary conditions at the two edges of each

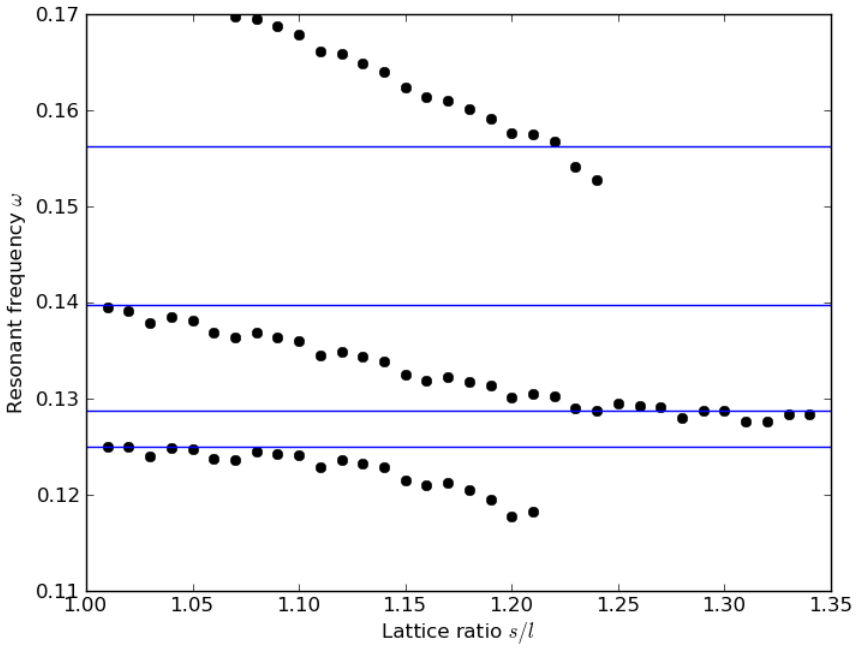

Figure 3.5: The resonant frequencies of the low order TE modes increase as the resonators couple more strongly, and there is a new mode below TE_{11}. The blues lines represent the 10, 11, 12, and 13 modes of the rectangular cavity of identical dimensions, which the microstrip resonator should resemble.

resonator are replaced by new conditions at the middle of the gaps between neighboring resonators. These new boundary conditions are obviously that the tangential electric fields should be at their maximum on the xy planes at each gap location. Equivalently, there should be zero tangential magnetic fields on these planes; these boundary conditions are simply the open circuit boundary conditions discussed above. The resonant modes take the form given by equations (2.23) - (2.25). Note that the coupled TE_{11} mode at $s/l \approx 1$ corresponds to $m = 1, n = 2$ in these equations. This notation will continue to be used, since this mode deforms continuously into the uncoupled TE_{11} mode and not the uncoupled TE_{12} mode.

As can be seen in (2.23) - (2.25), a third formulation of the coupled boundary conditions is that there should be zero normal electric field on the xy planes at the gaps. These boundary conditions make physics sense. The symmetry created by the two opposing edges

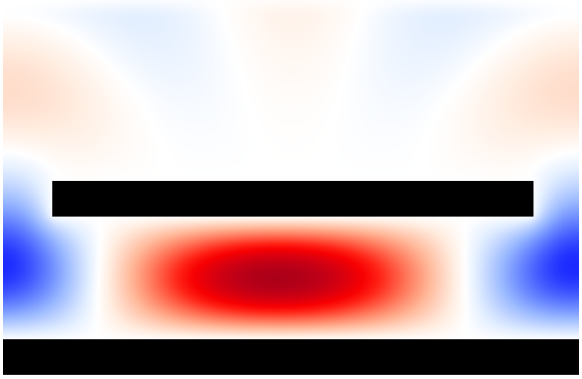

Figure 3.6: The resonant frequency of the TE_{11} mode begins to shift higher as the microstrip separation distance decreases ($s/l = 1.20$).

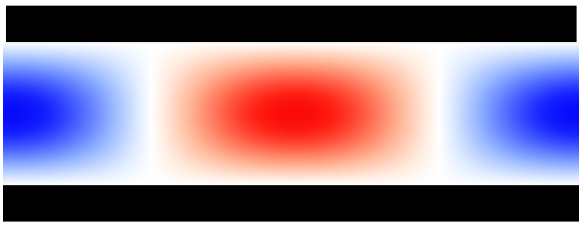

Figure 3.7: The TE_{11} mode has been perturbed to a degenerate mode with the same frequency as the uncoupled TE_{12} mode ($s/l = 1.01$).

of neighboring microstrips facing each other across the gap (see Fig. 3.4) implies that there should be no normal (symmetry-breaking) electric field in this gap. As the distance between neighboring resonators approaches zero, the 11 mode where initially $E_y \sim \sin \pi z/L'$ is perturbed until in the end $E_y \sim \cos 2\pi z/L$ (Fig. 3.7).

Additionally, a new mode is observed below the uncoupled TE_{10} frequency (Fig. 3.5). This cannot be a TE_{0x} mode, since these "modes" must take the value 0 everywhere in the waveguide. Moreover, this mode converges to the uncoupled TE_{10} mode in the same manner that TE_{11} converges to the uncoupled TE_{12}. By analogy, it will be called the $TE_{1,-1}$ mode. Several images of the electric field in this mode are shown in Figs. 3.9 and 3.10. Again, it is easy to make intuitive sense of this resonant mode. Before the gaps approach zero size, there are resonances located around each one. As the gaps decrease in size, these individual

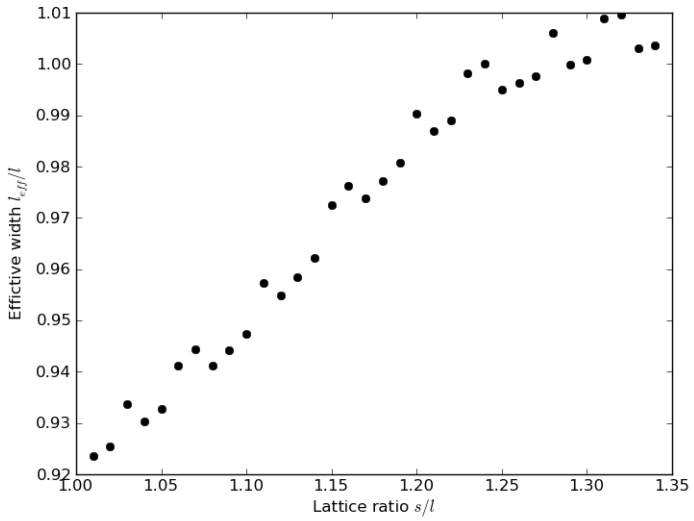

Figure 3.8: The increase is resonant frequency is numerically attributable to a decrease in the effective width of the microstrip resonator, although this isn't the most physical interpretation.

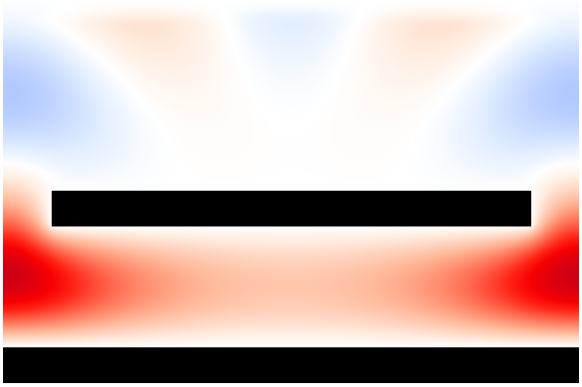

Figure 3.9: The $TE_{1,-1}$ mode appears once the gap becomes small enough that it is not too lossy ($s/l = 1.20$).

resonance combine until their magnitude is constant across z. This mode, the coupled $TE_{1,-1}$ mode in the limit $s/l \approx 1$, is described by (2.23) - (2.25) with $m = 1$ and $n = 0$ (so it is at the same frequency as the uncoupled TE_{10} of the rectangular cavity resonator).

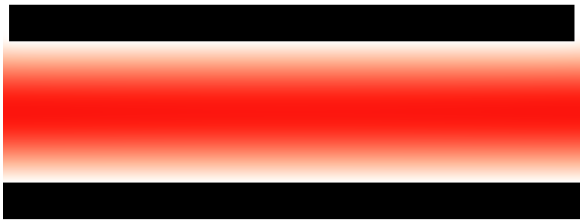

Figure 3.10: The TE_{1-1} is essentially identical to the uncoupled TE_{10} mode when $s/l \approx 1$ ($s/l = 1.01$).

3.3 Absorption Spectrum

Unfortunately, Meep is not capable of modeling a material with constant complex ϵ. Instead, any lossy material must be modeled with a Lorentzian function

$$\epsilon(\omega) = \left(1 + \frac{i\sigma_D}{\omega}\right)\left\{\epsilon_\infty + \sum_n \frac{\sigma_n \omega_n^2}{\omega_n^2 - \omega^2 - i\omega\gamma_n}\right\}, \tag{3.2}$$

where σ_D is a parameter representing conductivity and each triple $(\omega_n, \gamma_n, \sigma_n)$ characterizes a resonance at frequency ω_n with a width related to γ_n and a relative strength σ_n. Representing a flat and complex dielectric constant is a matter of gaming Meep's system. Take the task of modeling a dielectric constant $\epsilon = \epsilon_r + i\epsilon_i$. The simplest way to do so with only one Lorentzian term is to first let $\sigma_D = 0$ and $\epsilon_\infty = \epsilon_r$. Then let ω_0 be a frequency in the middle of the frequency range of interest (so that $\omega_0^2 - \omega^2$ is small) and let $\sigma_0 = \epsilon_i\gamma_0/\omega_0$. In the limit $\gamma_0 \to \infty$ (in Meep we can set $\gamma_0 = 10^{10}$ or some other arbitrarily high number), we have

$$\epsilon(\omega) = \epsilon_r + \frac{\epsilon_i\gamma_0\omega_0}{\omega_0^2 - \omega^2 - i\omega\gamma_0} \to \epsilon_r + i\epsilon_i\left(\frac{\omega_0}{\omega}\right). \tag{3.3}$$

This is not an ideal situation, but it the best that can be done without resorting to numerical approximations involving multiple Lorentzian terms (in fact, a least squares fit with just one Lorentzian term does barely any better). This numerical fit can be performed with a program

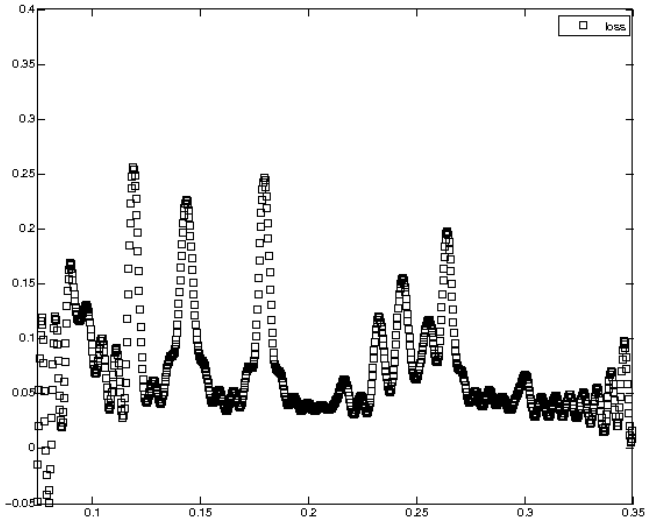

Figure 3.11: Absorption spectra of the microstrip resonator lattice on a broader frequency range shows rough correspondence to low order resonant modes of microstrip resonator ($s/l = 1.35$).

such as Mathematica, giving excellent results. A fit to the parameters $\epsilon_r = 1$ and $\epsilon_i = 0.5$ using Mathematica is given in the appendices (B.1). However, using these parameters within Meep caused numerical convergence issues for unknown reasons. Further research could try to modify these fits to work with Meep or use an alternate FDTD simulation program. For now, the less than ideal approximation given by (3.3) is used.

Using this approximation, Meep can simulate the absorption spectra of the lattice of two dimensional microstrip resonators. The file used to perform this simulation is shown in Appendix A.4. Fig. 3.11 shows the absorption spectra across a broad frequency range spanning the low order $1n$ and $2n$ modes. The peaks are not located exactly at the system's resonant frequencies (partly because the dielectric simulated is a function of frequency). However, they do appear to correspond roughly to these frequencies, with several peaks between $\omega = 0.12$ and 0.2 (in Meep units, as described above) corresponding to $1n$ modes

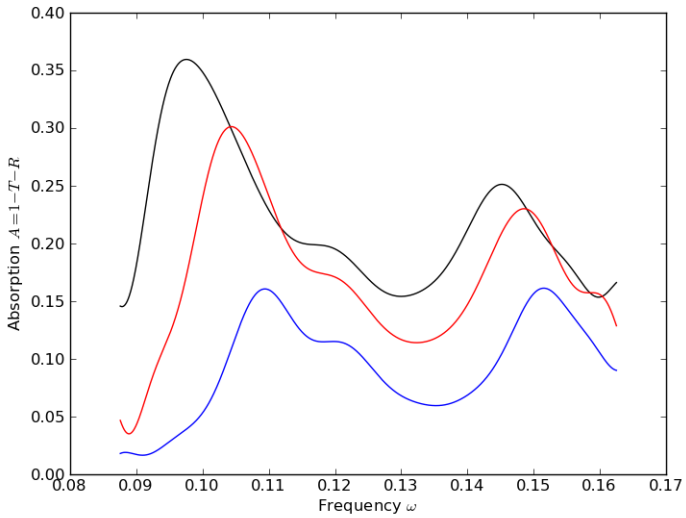

Figure 3.12: Absorption spectra of the microstrip resonator lattice (black line $s/l = 1.30$, red line $s/l = 1.25$, and blue line $s/l = 1.20$).

and a group of more tightly spaced peaks around $\omega = 0.25$ corresponding to $2n$ modes.

Figs. 3.12 shows the absorption in a narrower frequency band centered around the 10 and 11 modes as the spacing s/l between resonators is decreased. These plots show two peaks, the lower of which should contain the nearby $TE_{1,-1}$, TE_{10}, and TE_{11} modes, and the higher of which is around the TE_{13} mode. As the ratio s/l is decreased to 1 and the microstrip resonators are brought together, the absorption peaks rise in frequency along with the resonant modes, although they change in relative strength. These results clearly do not agree with the results of previous research that prompted this thesis, which found that the peak in absorption decreased in frequency as the microstrips were brought together. It is observed here that an unexpected absorption spike appears at the new resonant mode $TE_{1,-1}$. Perhaps in three dimensions, there is a continuous class of these extra resonant modes that accounts for the smooth transition to lower frequencies observed in earlier simulations.

Chapter 4

Analysis

4.1 Periodically Loaded Transmission Line

The transmission line literature treats transmission line coupling to resonators [6, pp. 564-72]. However, the manner in which it does so presupposes knowledge of the resonant modes of the resonator, and does not consider perturbations to these modes caused by coupling to the transmission line. Instead, in the limit where $s/l \approx 1$, the sequence of microstrip resonators can be treated as a periodically loaded transmission line with series capacitive elements. The equivalent circuit for this representation is shown in Fig. 4.1. Following a similar textbook example [2, pp. 230-233], consider the propagation of a wave along this transmission line. Let θ be the effective propagation from one cell to the next, i.e. $V_{n+1} = V_n e^{-i\theta}$ and $I_{n+1} = I_n e^{-i\theta}$. Let k be the propagation constant along each transmission line segment, treated as a two port with characteristic impedance $Z_0 = \sqrt{L/C}$. Then the transmission line equations (which imply that the current and voltage vary sinusoidally in between the capacitors) together with

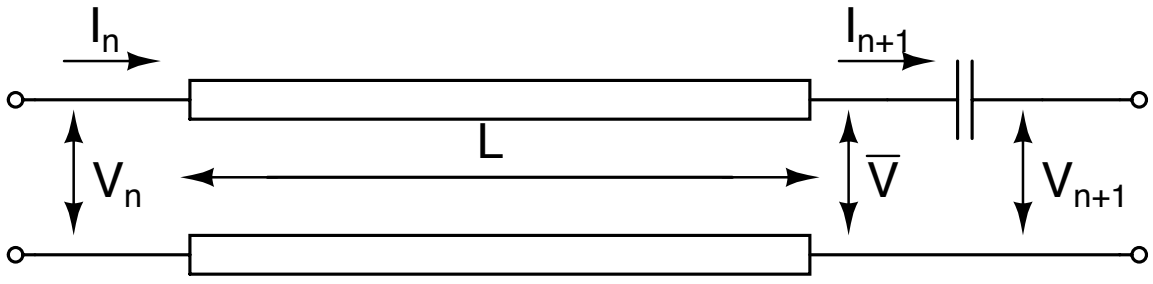

Figure 4.1: When the coupling between neighbors is large and the loss is low, the sequence of microstrip resonators behaves like a periodically capacitively loaded transmission line. Each segment of this transmission line can be represented by this characteristic two-port.

Kirchoff's laws give

$$V_{n+1} = V_n \cos k\ell - iZ_0 I_n \sin k\ell - \left(\frac{1}{i\omega C_0}\right) I_{n+1} \tag{4.1}$$

$$I_{n+1} = -iY_0 V_n \sin k\ell + I_n \cos k\ell \tag{4.2}$$

Substituting the θ propagation terms and multiplying the two equations yields (after a little big of algebra)

$$\cos\theta = \cos k\ell + \frac{Y_0}{2\omega C_0} \sin k\ell. \tag{4.3}$$

Physically, we are interested in the case where the coupling between the neighboring resonators is arbitrarily strong, i.e. $\omega C_0 \gg Y_0$. When length ℓ of transmission line segment (resonator) is near an integer multiple of half the wavelength, $k\ell \approx n\pi$ and $\cos k\ell \approx (-1)^n$. If n is odd and $\sin k\ell < 0$, then $\cos\theta < -1$ and there will be no real solution for θ. Similarly, when n is even and $\sin k\ell > 0$, there cannot be a real solution for θ. In general there are no real solutions for the propagation constant θ in the narrow frequency bands $n\pi < k\ell < n\pi + \Delta$ (where $\Delta \ll 1$).

This analysis supports the behavior seen in the simulations. The high capacitance gaps in the "transmission line" act as boundary conditions that create resonant conditions at certain frequencies. Waves at these frequencies cannot propagate through the transmission line because they become trapped inside the resonators, leading to the stop gaps in θ. The success of this transmission line model indicates that it might have the potential to describe the microstrip resonator system between the uncoupled and completely coupled ($\omega C_0 \gg Y_0$) limits.

4.2 Normal Mode Expansion

The gaps between successive microstrip resonators act as periodically spaced apertures on a microstrip transmission line (or, as a more manageable approximation, a parallel plate transmission line). As outlined in Jackson [1, pp. 398 - 294], such a model can be studied by assigning harmonic sources to the apertures and calculating the excited field inside the waveguide as a superposition of its orthonormal modes, i.e. the modes normalized such that

$$\int_A \mathbf{E}_m \cdot \mathbf{E}_n = \delta_n^m,$$

where A is a cross section of the waveguide. The orthonormal TM and TE normal modes can be calculated easily from (2.7) - (2.12). The components of the forward propagating mth orthonormal TM mode are

$$E_x = \sqrt{\frac{2}{a}} \cos\left(\frac{m\pi x}{a}\right) \tag{4.4}$$

$$H_y = \pm\frac{\epsilon\omega}{k_m}\sqrt{\frac{2}{a}} \cos\left(\frac{m\pi x}{a}\right) \tag{4.5}$$

$$E_z = \mp\frac{im\pi}{k_m a} \sin\left(\frac{m\pi x}{a}\right) \tag{4.6}$$

Similarly, the components of the forward propagating mth orthonormal TE mode are

$$H_x = \pm\frac{k_m}{\mu\omega}\sqrt{\frac{2}{a}} \sin\left(\frac{m\pi x}{a}\right) \tag{4.7}$$

$$E_y = \sqrt{\frac{2}{a}} \sin\left(\frac{m\pi x}{a}\right) \tag{4.8}$$

$$H_z = \frac{-im\pi}{\mu\omega a} \cos\left(\frac{m\pi x}{a}\right) \tag{4.9}$$

The total electromagnetic fields caused by the incident fields is the superposition of the forward propagating and backwards propagating fields that are excited, i.e. $\mathbf{E} = \mathbf{E}^{(+)} + \mathbf{E}^{(-)}$ [1, 8.137]. Each of these traveling waves can be given as a superposition of orthonormal modes

$$\mathbf{E}^{(\pm)} = \sum_{\lambda} A_{\lambda}^{(\pm)} \mathbf{E}_{\lambda}^{(\pm)}, \tag{4.10}$$

where λ is an index thats runs over all TE and TM orthonormal modes of the waveguide (given by (4.4) - (4.9)). In this particular case, where the waveguide is excited by a source at an aperture, the coefficients can be calculated using (8.147) from Jackson [1].

Consider a TE electric field applied at the apertures on the resonator sequence (Fig. 1.1), i.e. $E_y = E_0 e^{-i\omega t}$. Since the excitation is a TE mode, it turns out that it does not excite any TM modes of the waveguide. This excitation is compatible with the heuristic observations made of the resonant modes of the coupled resonator system (that the periodic gaps became boundaries at which the normal component of the electric field is forced to be zero; see above). Moreover, this case is much simpler than the corresponding TM case. The coefficients for the excited TE modes are determined using (8.147) from Jackson:

$$\begin{aligned} A_m^{(\pm)} &= \frac{Z_{TE}}{2} \int_A \left(\tilde{\mathbf{E}} \times \mathbf{H}_m^{(\mp)} \right) \cdot \hat{\mathbf{n}} \, dz \\ &= \frac{\mu\omega}{2k_m} \int_A \left(E_0 \cdot \frac{-i\gamma_m}{\mu\omega} \sqrt{\frac{2}{a}} e^{\mp i k_m z} \right) (\hat{\mathbf{y}} \times \hat{\mathbf{z}}) \cdot \hat{\mathbf{x}} \, dz \\ &= i E_0 \frac{\gamma_m}{2k_m} \sqrt{\frac{2}{a}} \int_a^b e^{\mp i k_m z} \, dz. \end{aligned}$$

Now take the points a and b to be the two end points of an aperture centered at $z = c$. The

integral term above becomes

$$\begin{aligned}\int_{c-d/2}^{c+d/2} e^{\mp ik_m z}\,dz &= \frac{1}{\mp ik_m} e^{\mp ik_m z}\Big|_{c-d/2}^{c+d/2} \\ &= \frac{1}{\mp ik_m}\left(e^{\mp ik_m(c+d/2)} - e^{\mp ik_m(c-d/2)}\right) \\ &= \frac{2e^{\mp ik_m c}}{k_m}\left(\frac{e^{\mp ik_m d/2} - e^{\pm ik_m d/2}}{\mp 2i}\right) \\ &= \frac{2\sin(k_m d/2)}{k_m} e^{\mp ik_m c}.\end{aligned}$$

Substituting these into (4.10) gives an an expression for the excited electric field as a superposition of normal modes of the waveguide. At first glance the resulting expression does not seem likely to convert. However, recall that each mode has a cutoff frequency below which it cannot propagate. A frequency ω can only excite propagating modes with real k_m when $m\pi/a < \sqrt{\mu\epsilon}\omega$. This ensures that only a finite number of propagating modes are excited. The non-propagating modes can then be safely ignored. With this caveat,

$$\begin{aligned}\mathbf{E} &= \sum_m A_m^{(+)}\mathbf{E}_m^{(+)} + \sum_m A_m^{(-)}\mathbf{E}_m^{(-)} \\ &= \sum_m \left\{\left(\frac{iE_0 m\pi}{k_m^2 a}\sqrt{\frac{2}{a}}\sin\left(\frac{k_m d}{2}\right)e^{-ik_m c}\right)\sqrt{\frac{2}{a}}\sin\left(\frac{m\pi x}{a}\right)e^{ik_m z}\hat{\mathbf{y}}\right\} \\ &\quad + \sum_m \left\{\left(\frac{iE_0 m\pi}{k_m^2 a}\sqrt{\frac{2}{a}}\sin\left(\frac{k_m d}{2}\right)e^{ik_m c}\right)\sqrt{\frac{2}{a}}\sin\left(\frac{m\pi x}{a}\right)e^{-ik_m z}\hat{\mathbf{y}}\right\} \\ &= \frac{4iE_0}{a^2}\sum_m \left\{\left(\frac{m\pi}{k_m^2}\sin\left(\frac{k_m d}{2}\right)\right)\sin\left(\frac{m\pi x}{a}\right)\cos\left(k_m(z-c)\right)\right\}\hat{\mathbf{y}}\end{aligned}$$

A particular segment of the waveguide is terminated by two apertures located at $c = L/2$ and $c = -L/2$. If these are the only two apertures present, the total electric field inside the waveguide can be found by superimposing the fields caused by each of these apertures. With the trigonometric relation $\cos(a+b) + \cos(a-b) = 2\cos a \cos b$, the total electric field

present in the waveguide is

$$E_y = \frac{8iE_0}{a^2} \sum_m \left(\frac{m\pi}{k_m^2} \sin\left(\frac{k_m d}{2}\right) \cos\left(\frac{k_m L}{2}\right) \right) \sin\left(\frac{m\pi x}{a}\right) \cos\left(k_m z\right) \tag{4.11}$$

The $\cos(k_m L/2)$ term regulating the magnitude of the excited field reaches its maximum magnitude when $k_m = 2n\pi/L$ for some integer n, i.e. when ω is the resonant frequency of a $\mathrm{TE}_{m,2n}$ mode of rectangular cavity resonator of dimensions (a, L). Furthermore, this resonant mode will be the dominant mode when the waveguide is excited at this frequency ω. Consider another (waveguide) with propagation factor $k_{\tilde{m}}$, where $\tilde{m} > m$. Physically, $a \ll L$, and so

$$k_{\tilde{m}}^2 = \left(\frac{2n\pi}{L}\right)^2 + \left(\frac{m\pi}{a}\right)^2 - \left(\frac{\tilde{m}\pi}{a}\right)^2 < 0 \tag{4.12}$$

Essentially, since a is much less than L the mode number describing periodicity in the direction of a has a much larger effect on the frequency and propagation of wave than the number describing periodicity in the direction L. Explicitly, when $\tilde{m} \sim n$, $1 \sim \tilde{m}/n \gg a/L$ and thus $\tilde{m}/a \gg n/L$, justifying (4.12). On the other hand, when $\tilde{m} < m$, the propagation factor $k_{\tilde{m}}$ is greater than k_m, and inspection of (4.11) shows that this mode does not contribute nearly as much to the total excited field. Since additionally $d \ll L$, the magnitude of the resulting electric field varies simply with respect to the geometric and mode parameters as

$$|E_y| \propto \left(\frac{m}{n}\right)\left(\frac{Ld}{a^2}\right) \tag{4.13}$$

These results agree to a degree with the simulated absorption spectra of the system of microstrip resonators. Normal mode analysis predicts that maximum absorption will occur when ω is the frequency of some mode, in fact a mode $\mathrm{TE}_{m,2n}$, of the system. This agrees completely with previous results, but the restriction of the second parameter to $2n$ (i.e. to even integers) has not been seen before. This does not necessarily contradict the simulations,

since the absorption spectra did not seem to have peaks at each resonant mode, and warrants further investigation. Secondly, normal mode analysis predicts that the strength of the excited field in the dielectric should be proportional to m/n. The simulations did seem to show decreasing resonant strength with n, though not increasing strength with m. Again, this is a target for further investigation.

4.3 Conformal Mapping

The analysis of fields around the gaps between neighboring microstrip resonators is possible using the techniques of conformal mapping. Conformal mapping can be used, for example, to analyze the fringing fields at the ends of a parallel plate capacitor, specifically by using the Schwarz transformation (see [6, pp. 345-348]). This leads to hope that the gap between the microstrip resonators, which is essentially a symmetric version of the parallel plate capacitor fringing problem, can be approached by similar means. However, a direct attempt to use the Schwarz transformation becomes unmanageable. Instead, consider the similar problem of finding the fringing fields between two disconnected parallel plate capictors, as shown in Fig. 4.2. Mathematically, this consists of solving Laplace's equation on the plane with boundary conditions in which two of the plates are grounded and the other two are at a potential V. This problem is treated in [4, p. 197], which gives the conformal map $f\colon \mathbb{D} \to \mathbb{C}$ from the unit disk (shown in Fig. 4.3) given by

$$w = f(z) = \frac{1}{2}\sin^2\alpha \log\left(\frac{1+z}{1-z}\right) + \frac{1}{2}\cos^2\alpha\left(\frac{2z}{1+z^2}\right) \tag{4.14}$$

Here, α is a constant such that $f(\exp i\alpha) = a + bi$, where the four boundaries are separated horizontally by a distance a and vertically by a distance b (so $(a + bi)/2$ is the complex

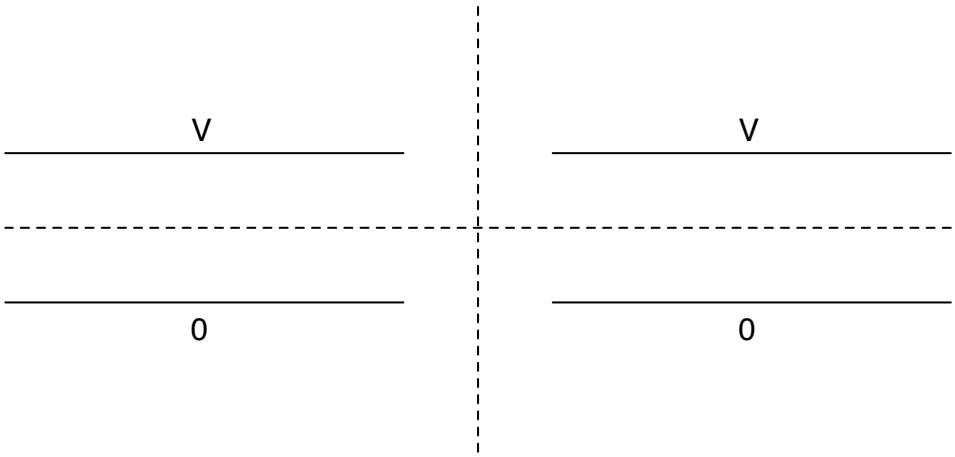

Figure 4.2: The electrostatic fields between two coupled microstrips (or simply parallel plate capacitors) are more easily found by making the problem symmetric with respect to both axes.

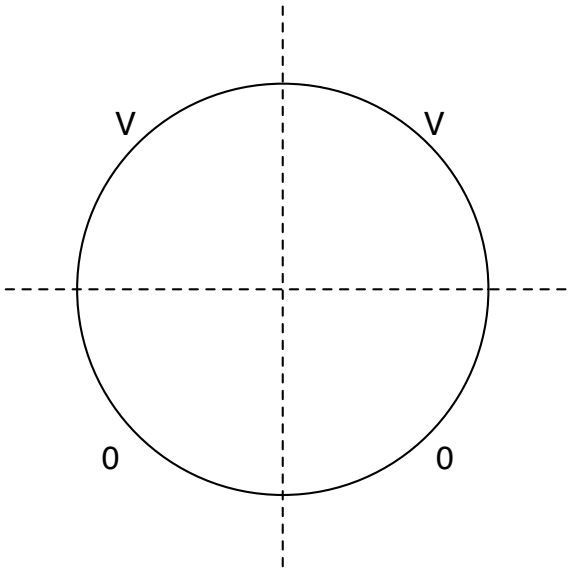

Figure 4.3: The unit disk $\mathbb{D}$ with these boundaries is conformally equivalent (via the map f) to the complex plane $\mathbb{C}$ with boundaries shown in Fig. 4.2.

coordinate of the end of the boundary in the first quadrant). The boundaries on the plane are mapped onto by the boundary of the unit circle in the obvious way (each being associated with its corresponding quadrant), as shown in Fig. 4.3. Laplace's equation is easier to solve on the unit disk, but only through the use of an infinite series of Bessel functions. Instead,

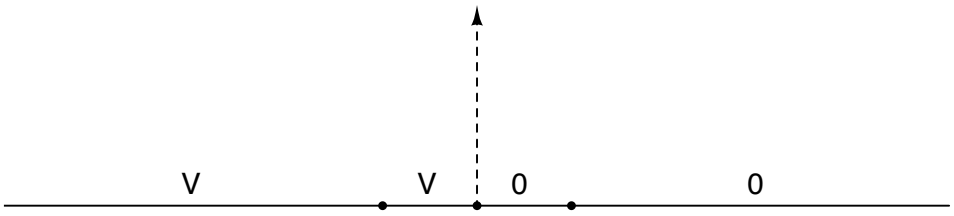

Figure 4.4: The upper half plane $\mathbb{H}$ is conformally equivalent (via the map g) to Fig. 4.2.

f can be modified into a conformal map from the complex upper half plane $\mathbb{H}$ onto $\mathbb{C}$ by composing it with the Cayley transform $z \mapsto (z-i)/(z+i)$, which maps the upper half plane onto the unit disk. The resulting map $g\colon \mathbb{H} \to \mathbb{C}$ is given by

$$w = g(z) = \frac{1}{2}\sin^2\alpha \log(-iz) + \frac{1}{2}\cos^2\alpha \left(\frac{z^2+1}{z^2-1}\right), \tag{4.15}$$

As shown in Fig. 4.4, the boundaries in $\mathbb{C}$ are the images of the pieces $(-\infty,-1)$, $(-1,0)$, $(0,1)$, and $(1,\infty)$ of the real axis in $\mathbb{H}$. Luckily, this works out such that Laplace's equation on the upper half plane $\mathbb{H}$ has boundary conditions V for $x<0$ and 0 for $x>0$. This problem is solved in [6, pp. 339-40] by introducing a transformation from $\mathbb{W} = \{z \in \mathbb{C}\colon 0 \leq \Im(z) \leq V\}$ to $\mathbb{H}$, given by $z \mapsto \exp(\pi z/V)$, that maps lines of constant imaginary part in $\mathbb{W}$ to equipotential lines in the $\mathbb{H}$ plane (which are mapped to equipotential lines in $\mathbb{C}$ by g). Combining this logarithmic transformation with (4.15), we arrive at the transformation $h\colon \mathbb{W} \to \mathbb{C}$ given by

$$w = h(z) = \frac{1}{2}\sin^2\alpha \left(\frac{\pi z}{V} - \frac{i\pi}{2}\right) + \frac{1}{2}\cos^2\alpha \coth\left(\frac{\pi z}{V}\right) \tag{4.16}$$

that takes each line $u + i\phi \subset \mathbb{W}$ to the equipotential lines at potential ϕ in the Fig. 4.2. A plot of these equipotential lines is shown in Fig. 4.5 (the constant α has been arbitrarily set to 1 for convenience).

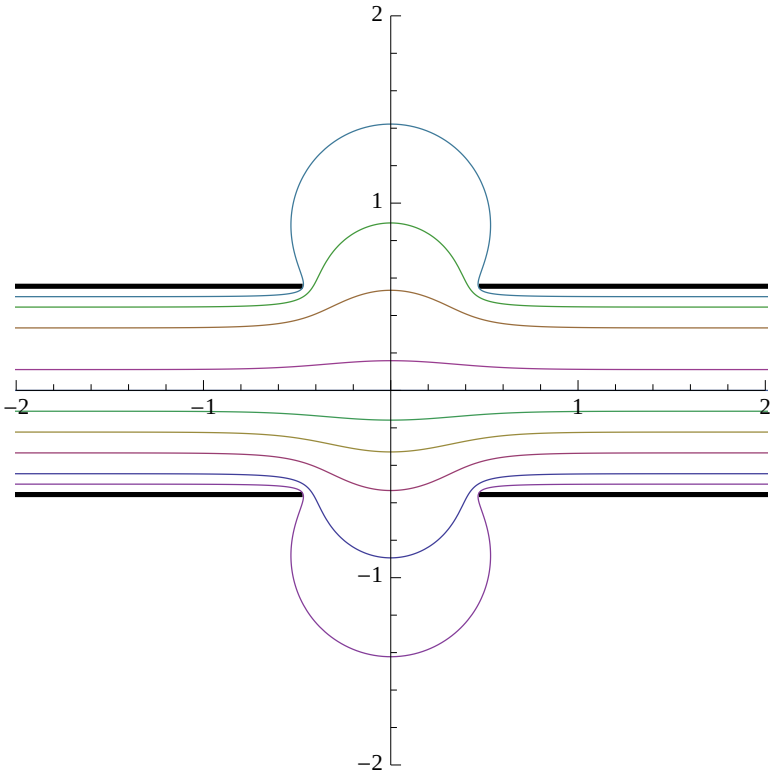

Figure 4.5: The equipotential lines for a static electromagnetic field between two microstrip resonators can be found with (4.16).

These equipotential lines do not, of course, give the solution to the wave equation around this area of the gap. As shown in [6, pp. 348-349], the conformal map h can be used to pull back the Helmholtz equation (describing the separated spatial component of a wave) in $\mathbb{C}$ to the region $\mathbb{W}$, on which the boundary shapes are lines of constant imaginary part. Letting u and v be the real and imaginary coordinates of the region $\mathbb{W}$ and letting $w = h(z)$, this equation is of the form

$$\nabla^2_{uv}\psi + \left|\frac{dw}{dz}\right|^2 k^2\psi = 0 \tag{4.17}$$

It is beyond the scope of this thesis to consider treating this equation, as it is complicated and quite likely impossible to solve analytically. There are perhaps regions where the equation can be solved at least approximately, aiding understanding of the coupling between two

microstrip resonators, and this is a possible avenue for further research.

Chapter 5

Conclusion

The results of the studies presented in this thesis were mixed. It was necessary for both computational reasons and analytical reasons to restrict focus to the 2D equivalent of a microstrip resonator. Neither simulation nor analysis showed the 2D resonator to behave in the manner that previous simulations suggested the 3D microstrip should. In fact, the 2D resonator had the opposite behavior - its resonant modes and absorption peaks increased in frequency as the neighboring microstrip resonators were coupled more strongly, rather than decrease in frequency. However, the observed behavior of the 2D resonators made physical sense and mostly agreed with the analytical results.

The results suggest several promising routes for further research. As mentioned, there are several areas in which the simulations and analyses presented here could be extended, such as fixing the dielectric model used in absorption simulation. Similarly, the normal mode expansion performed could be further analyzed to better understand the relationship between the absorption spectrum of the system and its resonant modes, and the conformal map derived could be used as the starting point of a more exact analysis of the propagation of fields between two resonators. With the better understanding of the behavior of microstrip resonators that has been gained from these simulations, the computational time cost of performing similar 3D simulations should be manageable. Other analogous physical problems not considered here could be simulated, such as the of a microstrip resonator coupled to two transmissions lines (a non-periodic problem) or studying the effect of the thickness of the microstrip on its modes and absorption spectrum.

Bibliography

[1] John David Jackson. *Classical Electrodynamics*. John Wiley & Sons, Inc., 3rd edition, 1999.

[2] Jin Au Kong. *Electromagnetic Wave Theory*. EMW Publishing, Cambridge, MA, 5th edition, 2005.

[3] V. A. Mandelshtam and H. S. Taylor. Harmonic inversion of time signals. *J. Chem. Phys.*, 107(17):6756 – 6769, 1997.

[4] Zeev Nehari. *Conformal Mapping*. International Series in Pure and Applied Mathematics. McGraw Hill Book Company, Inc., 1st edition, 1952.

[5] Ardavan F. Oskooi, David Roundy, Mihai Ibanescu, Peter Bermel, J. D. Joannopoulos, and Steven G. Johnson. Meep: A flexible free-software package for electromagnetic simulations by the FDTD method. *Computer Physics Communications*, 181:687–702, January 2010.

[6] Simon Ramo, John R. Whinnery, and Theodore Van Duzer. *Fields and Waves in Communication Electronics*. John Wiley & Sons, Inc., 3rd edition, 1994.

[7] Wheeler. Transmission-line properties of a strip on a dielectric sheet on a plane. *Microwave Theory and Techniques, IEEE Transactions on*, 25(8):631 – 647, 1977.

Appendix A
Meep Simulations

A.1 Rectangular Cavity Resonator

```
1  ; Using a=100nm convention
2
3  (define-param r 1.25)
4  (define-param l 16)
5  (define-param s (* l r))
6  (define-param w 4)
7  (define-param d (/ l 16))
8  (define-param dpml (/ s 16))
9  (define-param sx s)
10 (define-param sy s)
11 (define-param fcen 0.2)
12 (define-param df 0.3)
13 (define-param res 16)
14
15 (set-param! resolution res)
16 (set! eps-averaging? false)
17 (set! k-point (vector3 0 0 0))
18 (set! ensure-periodicity true)
19
20 (set! geometry-lattice (make lattice (size sx sy no-size)))
21 (define geom (list
22                 (make block
23                   (center 0 (/ (+ w d) 2))
24                   (size l d infinity)
25                   (material metal))
26                 (make block
27                   (center 0 (/ (+ w d) -2))
28                   (size l d infinity)
29                   (material metal))
30                 (make block
31                   (center (/ (+ l d) 2))
32                   (size d w infinity)
33                   (material metal))
34                 (make block
35                   (center (/ (+ l d) -2))
36                   (size d w infinity)
37                   (material metal))))
38
39 (set! geometry geom)
40
41 (set! pml-layers (list (make pml
42                          (thickness dpml))))
43
44 (set! sources (list (make source
```

```
45                      (src (make gaussian-src
46                             (frequency fcen)
47                             (fwidth df)))
48                      (component Ez)
49                      (center 0)
50                      (size 0 0))))
51
52 (use-output-directory)
53
54 (run-sources+ 100
55              (at-beginning output-epsilon)
56              (after-sources
57               (harminv Ez
58                        (vector3 0 0)
59                        fcen
60                        df)))
61
62 (run-until (/ 1 fcen)
63           (to-appended "ez" (at-every (/ 1 fcen 20) output-efield-z)))
```

A.2 Microstrip Resonator

```
1  ; Using a=100nm convention
2
3  (define-param r 1.25)
4  (define-param l 16)
5  (define-param s (* r l))
6  (define-param w 4)
7  (define-param d (/ s 16))
8  (define-param dpml (/ l 16))
9  (define-param sx s)
10 (define-param sy s)
11 (define-param fcen (/ 1 s pi))
12 (define-param df fcen)
13 (define-param nfreq 500)
14 (define-param res 16)
15
16 (set-param! resolution res)
17 (set! eps-averaging? false)
18 (set! k-point (vector3 0 0 0))
19 (set! ensure-periodicity true)
20
21 (set! geometry-lattice (make lattice (size sx sy no-size)))
22 (define geom (list
23                (make block
24                  (center 0 (/ (+ w d) 2))
25                  (size l d infinity)
26                  (material metal))
27                (make block
28                  (center 0 (/ (+ w d) -2))
```

```
29                  (size infinity d infinity)
30                  (material metal))))
31
32 (set! geometry geom)
33
34 (set! sources (list (make source
35                       (src (make gaussian-src
36                              (frequency fcen)
37                              (fwidth df)))
38                       (component Ez)
39                       (center 0 0)
40                       (size (/ w 2) (/ w 2)))))
41
42 (set! pml-layers (list (make pml
43                           (thickness dpml))))
44 (use-output-directory)
45
46 (run-sources+ 150
47               (at-beginning output-epsilon)
48               (after-sources
49                (harminv Ez
50                         (vector3 0 0)
51                         fcen
52                         df)))
53 (run-until (/ 1 fcen)
54            (to-appended "ez" (at-every (/ 1 fcen 20) output-efield-z)))
```

A.3 Periodic Microstrip Resonators

```
1  ; Using a=100nm convention
2
3  (define-param r 1.1)
4  (define-param l 16)
5  (define-param s (* l r))
6  (define-param w 4)
7  (define-param d (/ s 16))
8  (define-param dpml (/ s 16))
9  (define-param sx s)
10 (define-param sy s)
11 (define-param fcen (/ 1 s pi))
12 (define-param df fcen)
13 (define-param nfreq 500)
14 (define-param res 16)
15
16 (set-param! resolution res)
17 (set! eps-averaging? false)
18 (set! k-point (vector3 0 0 0))
19 (set! ensure-periodicity true)
20
21 (set! geometry-lattice (make lattice (size sx sy no-size)))
```

```
(define geom (list
                (make block
                  (center 0 (/ (+ w d) 2))
                  (size infinity d infinity)
                  (material metal))
                (make block
                  (center 0 (/ (+ w d) -2))
                  (size l d infinity)
                  (material metal))))

(set! geometry geom)

(set! sources (list (make source
                      (src (make gaussian-src
                             (frequency fcen)
                             (fwidth df)))
                      (component Ez)
                      (center 0.1 (/ w 3)))))

(set! pml-layers (list (make pml
                         (thickness dpml)
                         (direction Y))))
(use-output-directory)

(run-sources+ 100
              (at-beginning output-epsilon)
              (after-sources
               (harminv Ez
                        (vector3 0 0)
                        fcen
                        df)))
(run-until (/ 1 fcen)
           (to-appended "ez" (at-every (/ 1 fcen 20) output-efield-z)))
```

A.4 Lossy Periodic Resonators

```
; Using a=100nm convention

(define-param r 1.1)
(define-param l 16)
(define-param s (* l r))
(define-param w 4)
(define-param d (/ s 16))
(define-param dpml (/ s 16))
(define-param sx s)
(define-param sy s)
(define-param fcen (/ 1 s pi))
(define-param df fcen)
(define-param nfreq 500)
(define-param res 16)
```

```
15
16 (set-param! resolution res)
17 (set! eps-averaging? false)
18 (set! k-point (vector3 0 0 0))
19 (set! ensure-periodicity true)
20
21 (set! geometry-lattice (make lattice (size sx sy no-size)))
22 (define geom (list
23                 (make block
24                   (center 0 (/ (+ w d) 2))
25                   (size infinity d infinity)
26                   (material metal))
27                 (make block
28                   (center 0 (/ (+ w d) -2))
29                   (size l d infinity)
30                   (material metal))))
31
32 (set! geometry geom)
33
34 (set! sources (list (make source
35                       (src (make gaussian-src
36                              (frequency fcen)
37                              (fwidth df)))
38                       (component Ez)
39                       (center 0.1 (/ w 3)))))
40
41 (set! pml-layers (list (make pml
42                           (thickness dpml)
43                           (direction Y))))
44 (use-output-directory)
45
46 (run-sources+ 100
47               (at-beginning output-epsilon)
48               (after-sources
49                (harminv Ez
50                         (vector3 0 0)
51                         fcen
52                         df)))
53 (run-until (/ 1 fcen)
54            (to-appended "ez" (at-every (/ 1 fcen 20) output-efield-z)))
```

Appendix B
Mathematica Files

B.1 Flat Complex Epsilon Fit

freqs = Table[i, {i, 0.1, 0.2, 0.001}];
L = Length[freqs];
epsreal = Table[1.0, {i, 1, L}];
epsimag = Table[0.5, {i, 1, L}];
realdata = Transpose[{freqs, epsreal}];
imagdata = Transpose[{freqs, epsimag}];
epsexp = epsreal + I * epsimag;
model = $\epsilon + \sigma 1 * \omega 1\text{^}2/(\omega 1\text{^}2 - f\text{^}2 - f * I * \gamma 1) + \sigma 2 * \omega 2\text{^}2/(\omega 2\text{^}2 - f\text{^}2 - f * I * \gamma 2) +$
$\sigma 3 * \omega 3\text{^}2/(\omega 3\text{^}2 - f\text{^}2 - f * I * \gamma 3)$;
epsmodel = Table[model/.$f \to$ freqs[[i]], {i, 1, L}];
diffs = Table[epsmodel[[i]] − epsexp[[i]], {i, 1, L}];
MIN = Sum[Abs[diffs[[i]]]^2, {i, 1, L}];
LSQ = NMinimize[{MIN}, $\{\epsilon, \sigma 1, \omega 1, \gamma 1, \sigma 2, \omega 2, \gamma 2, \sigma 3, \omega 3, \gamma 3\}$]
$\{0.000162035, \{\epsilon \to 0.696189, \sigma 1 \to -0.349479, \omega 1 \to -0.343672, \gamma 1 \to -1.17164, \sigma 2 \to$
$0.348749, \omega 2 \to -0.423157, \gamma 2 \to 0.408676, \sigma 3 \to 0.431395, \omega 3 \to 0.260096, \gamma 3 \to 0.969677\}\}$
F[f_] = model/.LSQ[[2]];
Show[ListPlot[realdata, AxesOrigin $\to \{0.1, 0\}$],
Plot[Re[$F[f]$], {f, freqs[[1]], freqs[[L]]}, AxesOrigin $\to \{0.1, 0\}$]]

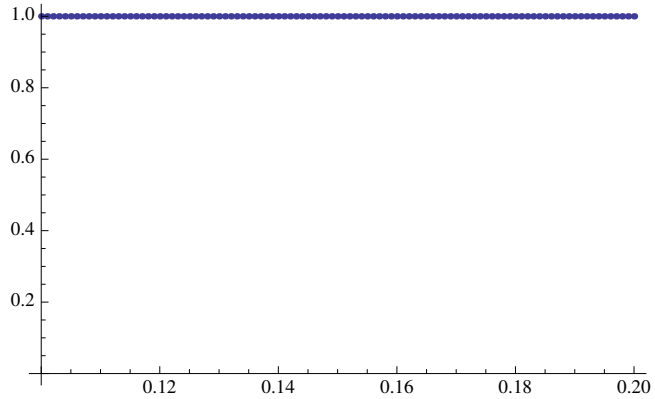

Show[ListPlot[imagdata, AxesOrigin $\to \{0.1, 0\}$],
Plot[Im[$F[f]$], {f, freqs[[1]], freqs[[L]]}, AxesOrigin $\to \{0.1, 0\}$]]

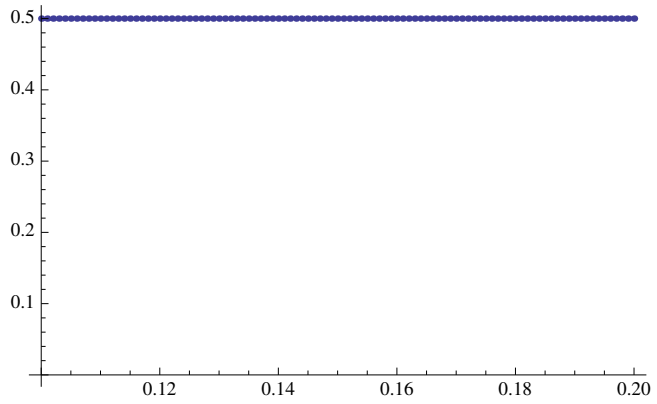

B.2 Conformal Map

$V = 1;$
$W[\text{z\_}] = 1/2 * \text{Sin}[\alpha]\text{^}2 * \text{Log}[(1+z)/(1-z)] + z * \text{Cos}[\alpha]\text{^}2/(1+z\text{^}2);$
$\text{W3}[\text{z\_}] = 1/2 * \text{Sin}[\alpha]\text{^}2 * (\text{Pi} * z/V - I * \text{Pi}/2) + 1/2 * \text{Cos}[\alpha]\text{^}2 * \text{Coth}[\text{Pi} * z/V];$
α:=1
$a = \text{Re}[N[W[\text{Exp}[I * \alpha]]]];$
$b = \text{Im}[N[W[\text{Exp}[I * \alpha]]]];$
$\text{W3C}[\text{x\_}, \text{y\_}] = \{\text{Re}[\text{W3}[x + I * y]], \text{Im}[\text{W3}[x + I * y]]\};$
$P = \text{ParametricPlot}[\{\{a + x, b\}, \{a + x, -b\}, \{-a - x, b\}, \{-a - x, -b\}\},$
$\{x, 0, 2\}, \text{AxesOrigin} \to \{0, 0\}, \text{PlotRange} \to \{-2, 2\},$
$\text{PlotStyle} \to \text{Directive}[\text{Black}, \text{Thick}]];$
$\text{Show}[P, \text{ParametricPlot}[\{\text{W3C}[0.05, x], \text{W3C}[0.1, x], \text{W3C}[0.2, x],$
$\text{W3C}[0.3, x], \text{W3C}[0.4, x], \text{W3C}[-0.05, x], \text{W3C}[-0.1, x], \text{W3C}[-0.2, x],$
$\text{W3C}[-0.3, x], \text{W3C}[-0.4, x]\}, \{x, 0, 1\}, \text{AxesOrigin} \to \{0, 0\},$
$\text{PlotRange} \to \text{All}]]$

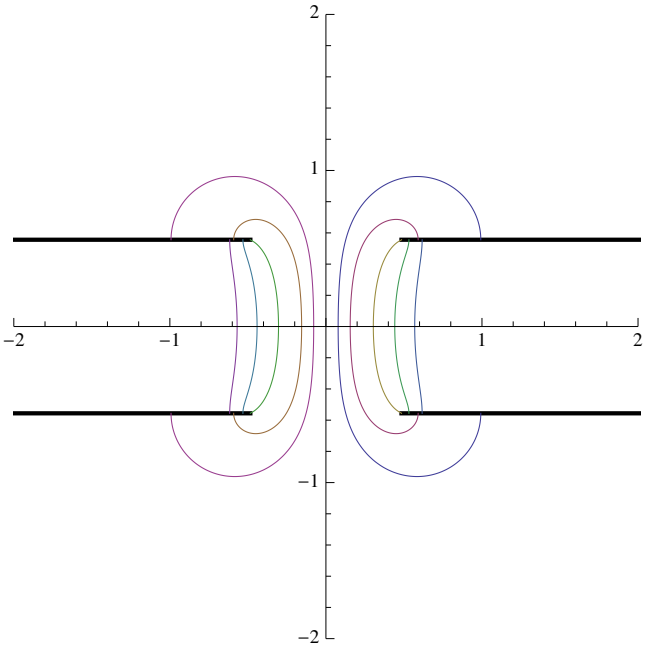

Show[P,
ParametricPlot[{W3C[x, 0.1], W3C[x, 0.2], W3C[x, 0.3], W3C[x, 0.4],
W3C[x, 0.5], W3C[x, 0.6], W3C[x, 0.8], W3C[x, 0.9], W3C[x, 0.95],
W3C[x, 0.05]}, {x, −2, 2}, AxesOrigin → {0, 0}, PlotRange → All]]